Probing gauge-mediated supersymmetry breaking models at the Fermilab Tevatron via delayed decays of the lightest neutralino

C.-H. Chen and J. F. Gunion
Department of Physics, University of California, Davis, California
(Received 6 February 1998; published 2 September 1998)

We quantitatively explore, in the context of the D0 detector at the Fermilab Tevatron, three very different techniques for observing delayed decays of the lightest neutralino of a simple gauge-mediated supersymmetry breaking (GMSB) model to photon plus gravitino. It is demonstrated that the delayed-decay signals considered can greatly increase the region of general GMSB parameter space for which supersymmetry can be detected. In the simple class of models considered, the combination of standard supersymmetry signals and delayed-decay signals potentially yields at least one viable signal for nearly all of the theoretically favored parameter space. The importance, for delayed-decay signal detection, of particular detector features and of building a simple photon detector on the roof of the D0 detector building is studied. [S0556-2821(98)00519-0]

PACS number(s): 12.60.Jv, 13.85.Qk, 14.80.Ly

I. INTRODUCTION

Even in the context of the minimal supersymmetric model (MSSM), it has become increasingly apparent that there are many different ways in which supersymmetry breaking can occur, leading to many different possible phenomenologies. In particular, gauge-mediated supersymmetry breaking (GMSB) models have attracted a great deal of interest in the last few years. The theory of gauge-mediated supersymmetry breaking posits that supersymmetry breaking is transmitted to the supersymmetric partners of the standard model (SM) particles via the SU(3)×SU(2)×U(1) gauge forces. Two GMSB model-building approaches have been explored in the literature.

In hidden-sector models, the GMSB model consists of three distinct sectors: a hidden sector where supersymmetry is broken, a ''messenger'' sector containing a singlet field and messenger fields with SU(3)×SU(2)×U(1) quantum numbers, and a sector containing the fields of the MSSM [1]. The coupling of the messengers to the hidden sector generates supersymmetry-breaking in the messenger sector.

In models of ''direct gauge mediation'' (sometimes called direct-transmission models) [2], the GMSB model consists only of two distinct sectors: a sector which is not only responsible for supersymmetry breaking but also contains the messenger fields, and the sector of MSSM fields.

In both classes of models, supersymmetry-breaking is transmitted to the MSSM sector via the SM SU(3)×SU(2)×U(1) gauge interactions between messenger fields and the MSSM fields. In particular, soft-supersymmetry-breaking masses for the gauginos and squared-masses for the squarks and sleptons arise, respectively, from one-loop and two-loop diagrams involving the virtual exchange of messenger fields.

Let us consider further the simple hidden-sector models of the first class in which the communication of supersymmetry breaking in the hidden sector to the messenger sector occurs via two-loop interactions involving a new gauge group with coupling g_m and in which the messenger sector consists of an SU(5) singlet superfield $\hat{S}$ and a certain effective number N_m of complete SU(5) representations. In such models the boundary conditions for the soft-supersymmetry-breaking masses are set at the mass scale of the messenger sector M_m and take a particularly simple form. For the gaugino Majorana mass terms one finds [1]

$$M_i(M_m) = k_i N_m g\left(\frac{\Lambda}{M_m}\right) \frac{\alpha_i(M_m)}{4\pi}\Lambda, \tag{1}$$

where $k_2 = k_3 = 1$, $k_1 = 5/3$ and $N_m \leqslant 4$ is required to avoid Landau poles. $\Lambda = \langle F_S\rangle/\langle S\rangle$ is the ratio of the vacuum expectation values of the auxiliary and scalar field components of the chiral field $\hat{S}$. Note that the gaugino masses have the same relative values as if they were unified at the grand-unification scale M_U even though the actual initial conditions are set at scale M_m. In addition, scalar masses are expected to be flavor independent since the mediating gauge forces are flavor-blind. In the simple models we consider here, they take the form

$$m_i^2(M_m) = 2\Lambda^2 N_m f\left(\frac{\Lambda}{M_m}\right)\sum_{i=1}^{3} c_i\left(\frac{\alpha_i(M_m)}{4\pi}\right)^2, \tag{2}$$

with $c_3 = 4/3$ (for color triplets), $c_2 = 3/4$ (for weak doublets) and $c_1 = \frac{5}{3}(Y/2)^2$ (in the normalization where $Y/2 = Q - T_3$). To avoid negative mass-squared for bosonic members of the messenger sector $M_m/\Lambda > 1$ is required; $M_m/\Lambda \geqslant 1.1$ is preferred to avoid fine-tuning, for which $f(\Lambda/M_m) \simeq 1$ and $1 \leqslant g(\Lambda/M_m) \leqslant 1.23$. For $M_m/\Lambda \geqslant 2$, $1 \leqslant g(\Lambda/M_m) \leqslant 1.045$. Here, we will consider masses obtained with $g = f = 1$. The results above at scale M_m must be evolved down to the scale of the actual sparticle masses, denoted Q. The resulting gaugino masses are given by replacing $\alpha_i(M_m)$ in Eq. (1) by $\alpha_i(Q)$. Evolution of the sfermion masses is detailed in Ref. [17]. Most important is the ratio $m_{\tilde{\ell}_R}/M_1 = \sqrt{6/5}\sqrt{r_1/N_m - (5/33)(1-r_1)}$, where $r_1 = (\alpha_1(M_m)/\alpha_1(Q))^2$. For the very broad range of $Q \geqslant m_Z$ and $M_m \leqslant 3\times 10^6$ TeV, $1 < r_1 \lesssim 1.5$, in which case the lightest of the sparticle partners of the SM particles is the $\tilde{\chi}_1^0 \sim \tilde{B}$ for

$N_m=1$ or the $\tilde{\tau}_R$ (more precisely, the $\tilde{\tau}_1$) for $N_m\geq 2$. Our numerical results are obtained by evolving from $M_m=1.1\Lambda$.

As for the other parameters of low-energy supersymmetry, the A-parameters (describing tri-linear Higgs-squark-squark and Higgs-slepton-slepton couplings) are suppressed, while the generation of the μ and B parameters (responsible for mixing of the Higgs superfields and scalar fields, respectively) is quite model-dependent (and lies somewhat outside the standard ansatz of gauge-mediated supersymmetry breaking). In the end, the parameters of the minimal GMSB model [3] consist of the normal 18 standard model parameters and three new parameters: Λ, $\tan\beta=v_u/v_d$ (the ratio of the vacuum expectation values of the neutral members of the Higgs doublet fields, H_u and H_d, responsible for giving mass to up-type and down-type quark fields, respectively) and sign(μ). This is the result after trading in the B and $|\mu|^2$ parameters for $v^2=v_u^2+v_d^2$ and $\tan\beta$, and using the observed value of m_Z to fix v. For this study, we have taken $\tan\beta=2$ and sign(μ)$=-1$. Further, we will consider only $N_m=1$ models in this paper.

The masses of the sparticles as a function of Λ, resulting from the above inputs, are easily summarized. For $N_m=1$ we have the following approximate rules of thumb when Λ is of order 100 TeV:

$$m_{\tilde{\chi}_1^0}\sim 1.35\ \text{GeV}\times\Lambda(\text{TeV}),\quad m_{\tilde{\chi}_1^+}\sim 2.7\ \text{GeV}\times\Lambda(\text{TeV}),$$
$$m_{\tilde{g}}\sim 8.1\ \text{GeV}\times\Lambda(\text{TeV}),\quad m_{\tilde{\ell}_R}\sim 1.7\ \text{GeV}\times\Lambda(\text{TeV}),$$
$$m_{\tilde{\ell}_L}\sim 3.5\ \text{GeV}\times\Lambda(\text{TeV}),\quad m_{\tilde{q}}\sim 11\ \text{GeV}\times\Lambda(\text{TeV}), \tag{3}$$

where M_1 is the U(1)-gaugino soft-supersymmetry-breaking mass, $m_{\tilde{g}}$ is the gluino mass, $m_{\tilde{q}}$ is a typical u or d squark mass, and $m_{\tilde{\ell}_R}, m_{\tilde{\ell}_L}$ are the masses of the right- and left-handed sleptons (all evaluated at the appropriate $Q\leq 1$ TeV). The masses of various sparticles in the case of $N_m=1$ are plotted as a function of Λ (taking $f=g=1$) in Fig. 1.

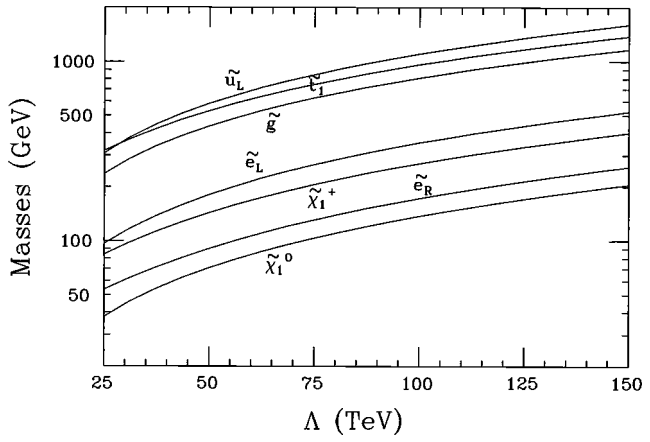

FIG. 1. $m_{\tilde{g}}$, $m_{\tilde{t}_1}$ and $m_{\tilde{u}_L}$ as functions of Λ in the $N_m=1$ GMSB scenario, taking $f=g=1$ and $M_m=1.1\Lambda$.

The range of Λ of interest in this model is easily determined using the dependence of the sparticle masses on Λ. An approximate upper limit is set by requiring that all superpartner masses be $\lesssim 1.5$ TeV. An approximate lower limit comes from requiring that the right-handed slepton be heavier than the rough lower limit of $\sim 70-80$ GeV from current data from the CERN e^+e^- collider LEP-2 [8] (see later discussion). From Fig. 1 and Eq. (3), we see that Λ values below 50–60 TeV would yield too small a value for $m_{\tilde{\ell}_R}$. For Λ values above about 150 TeV the squarks and gluino would have masses of order 1.5 TeV, which is somewhat beyond the range for which the model would provide a comfortable solution to the naturalness problem.

Assuming that supersymmetry is spontaneously broken in the hidden sector [4,5], a massless Goldstone fermion, the *Goldstino*, arises. Its coupling to a particle and its superpartner is fixed by the supersymmetric Goldberger-Trieman relation:

$$\mathcal{L}_{\text{int}}=-\frac{1}{F}j^{\mu\alpha}\partial_\mu\tilde{G}_\alpha+\text{H.c.}, \tag{4}$$

where $j^{\mu\alpha}$ is the supercurrent, which depends bilinearly on all the fermion–boson superpartner pairs of the theory and $\tilde{G}_\alpha$ is the spin-1/2 Goldstino field (with spinor index α). $\sqrt{F}$ is the scale at which supersymmetry-breaking occurs in the hidden sector. When gravitational effects are included, the Goldstino is ''absorbed'' by the *gravitino* ($\tilde{g}_{3/2}$), the spin-3/2 partner of the graviton. By this super-Higgs mechanism, the Goldstino is removed from the physical spectrum and the gravitino acquires a mass ($m_{3/2}$). In models where the gravitino mass is generated at tree-level one finds

$$m_{3/2}=\frac{F}{\sqrt{3}M_{\text{P}}}, \tag{5}$$

where M_{P} is the reduced Planck scale [$M_{\text{P}}=(8\pi G_N)^{-1/2}\sim 2.4\times 10^{18}$ GeV]. The helicity $\pm\frac{1}{2}$ components of the gravitino behave approximately like the Goldstino, whose couplings to particles and their superpartners are determined by Eq. (4). In contrast to the helicity $\pm\frac{3}{2}$ components of the gravitino couple with gravitational strength to particles and their superpartners, and thus can be neglected. It is convenient to rewrite Eq. (5) for the gravitino mass as follows:

$$m_{3/2}=\frac{F}{\sqrt{3}M_{\text{P}}}\sim 2.5\left(\frac{\sqrt{F}}{100\ \text{TeV}}\right)^2\ \text{eV}. \tag{6}$$

In the models we consider, the gravitino will be the lightest supersymmetric partner. The $\tilde{\chi}_1^0$ and $\tilde{\tau}_1$ will be substantially heavier; whichever of these two particle is the lighter will be called the next-to-lightest supersymmetric particle (NLSP), and will decay to the gravitino and its SM partner. If R-parity is conserved, as we assume, the gravitino will then be stable and thus will be a candidate for dark matter. If the gravitino lightest supersymmetric particle (LSP) is too heavy ($m_{3/2}\gtrsim$ few keV) its relic density will overclose the universe in most cosmological scenarios [6,7]. From Eq. (6),

this means that $\sqrt{F}$ values above roughly 3000 TeV are disfavored. On the other hand, there is no particular problem with very light gravitinos (eV masses). Although these will not contribute significantly to the total mass density of the universe, it may turn out that the main component of the dark matter has another source. Some examples are the QCD axion, its supersymmetric partner (the axino [9]) or the lightest stable particle in the GMSB messenger sector [10].

The scale of supersymmetry breaking, $\sqrt{F}$, is a very crucial parameter for the phenomenology of GMSB models. However, it is highly model-dependent. In hidden-sector models, values of $\sqrt{F}\sim 10^3-10^4$ TeV are required in order to generate sufficiently large supersymmetry-breaking in the sector of MSSM fields [11,7]. In particular, one can derive [11] the approximate inequality

$$\left(\frac{\sqrt{F}}{2000\ \text{TeV}}\right) \geqslant f\left(\frac{m_{\tilde{\ell}_R}}{100\ \text{GeV}}\right)\left(\frac{1}{27.5\sqrt{N_m}}\right), \tag{7}$$

where $f=F/F_S\sim(g_m^2/16\pi^2)^{-2}\sim 2.5\times 10^4/g_m^4$, with g_m being the coupling of the gauge group responsible for communicating (via two-loop diagrams) supersymmetry breaking from the hidden sector to the messenger sector. Perturbativity would require $g_m \lesssim 1$. For $m_{\tilde{\ell}_R}\geqslant 75-80$ GeV (the rough CERN e^+e^- collider LEP-2 limit) and $f=2.5\times 10^4$, Eq. (7) yields $\sqrt{F}\geqslant 10^4$ TeV ($\sqrt{F}\geqslant 5000$ TeV) for $N_m=1$ ($N_m=4$). Thus, even allowing for roughly a factor of 2 or 3 uncertainty in the approximate lower bound, $\sqrt{F}$ must lie near its upper limit from cosmology. In direct-transmission models, the two-loop communication between the hidden and messenger sectors is eliminated, f in Eq. (7) is effectively of order unity, and $\sqrt{F}$ can be as low as 100 TeV in phenomenologically viable models.

In what follows, we will focus on the ($N_m=1$) model in which the $\tilde{\chi}_1^0$ is the next-to-lightest supersymmetric particle.[1] We will employ the specific input boundary conditions given earlier. With these inputs, the model is completely specified in terms of just two independent parameters, Λ and $\sqrt{F}$. As explained above, Λ determines the gaugino and sfermion masses, while $\sqrt{F}$ determines the properties of the gravitino and (see below) the lifetime of the $\tilde{\chi}_1^0$. For $\sqrt{F}$ in the 100–3000 TeV range, the small size of the couplings, Eq. (4), imply that all the sparticles other than the $\tilde{\chi}_1^0$ undergo chain decay down to the $\tilde{\chi}_1^0$. The $\tilde{\chi}_1^0$ finally decays to a two-body final state containing the $\tilde{g}_{3/2}$. $\tilde{\chi}_1^0\to\gamma\tilde{g}_{3/2}$ is the only allowed two-body mode for $\Lambda\lesssim 80$ TeV, and this mode remains dominant out to the highest Λ values considered.[2] The $c\tau$ for $\tilde{\chi}_1^0\to\gamma\tilde{g}_{3/2}$ decay takes the form

$$(c\tau)_{\tilde{\chi}_1^0=\tilde{B}\to\gamma\tilde{g}_{3/2}}\sim 130\left(\frac{100\ \text{GeV}}{m_{\tilde{\chi}_1^0}}\right)^5\left(\frac{\sqrt{F}}{100\ \text{TeV}}\right)^4 \mu\text{m}. \tag{8}$$

If $\sqrt{F}\sim 3000$ TeV (the upper limit from cosmology), then $c\tau\sim 100$ m for $m_{\tilde{\chi}_1^0}=100$ GeV; $\sqrt{F}\sim 100$ TeV implies a short but vertexable decay length. Thus, the signatures for this GMSB model are crucially dependent on $\sqrt{F}$. In particular, for large $f=F/F_S$, and hence large $\sqrt{F}$, the neutralino decay is most naturally characterized by a substantial decay length, possibly of order tens to hundreds of meters. Events in which one or more of the neutralinos travels partway through the detector, and then decays, can be a substantial fraction of the total, as can events in which all the neutralinos exit the detector before decaying. Thus, at the very least, it is highly relevant to assess how our ability to discover supersymmetry changes as a function of $\sqrt{F}$. In the following sections of this paper we will focus on this issue in the context of the D0 detector at the Fermilab Tevatron collider.

Before proceeding with the Fermilab Tevatron analysis, let us return to the question of what the current CERN e^+e^- LEP-2 limits are upon the simple GMSB model we are considering. The latest limits [8] including $\sqrt{s}=183$ GeV running are quite significant, at least in the limits of either small $\sqrt{F}$ (for which $\tilde{\chi}_1^0\to\gamma\tilde{g}_{3/2}$ is prompt) or large $\sqrt{F}$ (for which the $\tilde{\chi}_1^0$ is invisible). In the small $\sqrt{F}$/prompt-photon limit, slepton mass limits of $\gtrsim 75-80$ GeV arise from looking for $\tilde{\ell}_R\tilde{\ell}_R$ events where $\tilde{\ell}_R\to\ell\tilde{\chi}_1^0\to\ell\gamma\tilde{g}_{3/2}$. Further, $m_{\tilde{\chi}_1^0}\gtrsim 80$ GeV is required by the absence of excess $\gamma\gamma+\not{E}_T$ events. In combination, these require $\Lambda\gtrsim 60$ TeV (see Fig. 1). In the large $\sqrt{F}$/invisible-$\tilde{\chi}_1^0$ limit, the normal supersymmetry (SUSY) search for $\tilde{\ell}_R\tilde{\ell}_R$ with $\tilde{\ell}_R\to\ell\tilde{\chi}_1^0$ implies $m_{\tilde{\ell}_R}\gtrsim 80$ GeV, implying $\Lambda\gtrsim 55$ TeV. The case of intermediate $\sqrt{F}$ has not yet been specifically analyzed, but we would anticipate that (conservatively) $\Lambda\lesssim 50-55$ TeV would be excluded by such an analysis. Thus, as stated earlier, we shall focus our analysis on the $\Lambda\gtrsim 50-60$ TeV region.

Finally, we wish to caution that many alternative GMSB models have now been constructed. In particular, the various direct-transmission models are very different from one another and need not have the simple M_m-scale boundary conditions of Eqs. (1) and (2). The relations between sparticle and gravitino masses vary tremendously. As an extreme ex-

[1]Focus on this model was originally motivated by the $ee\gamma\gamma$ event at the Tevatron [19]. However, recent Fermilab Tevatron analyses [20] rule out most, if not all, of the parameter space for which this model could have explained this event.

[2]The other two-body modes that become kinematically allowed at high Λ are $\tilde{\chi}_1^0\to Z\tilde{g}_{3/2}$ and $\tilde{\chi}_1^0\to h^0\tilde{g}_{3/2}$. However, for a $\tilde{\chi}_1^0$ that is nearly pure B-ino, the $\tilde{\chi}_1^0\to Z\tilde{g}_{3/2}$ width is suppressed relative to that for $\tilde{\chi}_1^0\to\gamma\tilde{g}_{3/2}$ by a factor of $[\sin\theta_W/\cos\theta_W]^2$ and the $\tilde{\chi}_1^0\to h^0\tilde{g}_{3/2}$ partial width is proportional to the square of the very small Higgsino component of the $\tilde{\chi}_1^0$.

ample, in the model of Ref. [12] the gluino is the LSP and the gravitino is sufficiently heavy as to be phenomenologically irrelevant.

The remainder of the paper is organized as follows. In Sec. II, we describe in detail the phenomenology of the $\tilde{\chi}_1^0$-LSP model and give results for all the signals considered. In particular, we describe in detail the delayed $\tilde{\chi}_1^0$ decay signals and illustrate the regions of model parameter space for which they would allow detection of a supersymmetry signal. Section III presents discussion and conclusions.

II. COLLIDER PHENOMENOLOGY

In the Introduction, we emphasized that our ability to detect supersymmetry at the Tevatron will depend substantially on $\sqrt{F}$. The case where $\sqrt{F}$ is sufficiently small that all $\tilde{\chi}_1^0$ decays are prompt received early attention [13,14,3,15,16]. Of these references, only [15] performs a quantitative Fermilab Tevatron collider study with the full boundary condition constraints of Eqs. (1) and (2). The results of Ref. [15] were confirmed in Ref. [18]. In these latter analyses, the prompt-decay hadron collider signal for supersymmetry considered was events containing two or more isolated photons, deriving from decay of two or more neutralinos, plus missing energy (and possibly other particles). The case where $\sqrt{F}$ is very large and most $\tilde{\chi}_1^0$ decays occur outside the detector was first analyzed in Ref. [18]; it is equivalent to conventional supersymmetry phenomenology (in which, for example, one looks for jets plus missing energy or three leptons plus missing energy) with the constraints implied by Eqs. (1) and (2) among the sparticle masses. For moderate $\sqrt{F}$, it is most appropriate to look for signals that would be characteristic of events in which the $\tilde{\chi}_1^0$ decay is delayed, but still occurs within the detector (or within a region that could be probed by a simple addition to the detector). In Ref. [18] one signal of this type was examined in the context of the D0 detector: namely, the ''outer-hadronic-calorimeter'' (OHC) signal that results when the delayed decay takes place in one of the outermost D0 hadronic calorimeter cells. Here, we will consider, in addition, two other delayed-decay signals. The first is the ''impact parameter'' (b) signal. If the (transverse) impact parameter of a photon appearing in the electromagnetic calorimeter could be shown to be non-zero, this would constitute a signal for a delayed decay. The extent to which the resolution for such an impact parameter measurement by the Collider Detector at Fermilab (CDF) and D0 detectors is adequate for this signal to be useful is an important issue. The second is the ''roof-array'' (RA) signal. For large $\sqrt{F}$, many $\tilde{\chi}_1^0$ decays will occur outside the muon chambers. A two-layer detector placed on the roof of the D0 detector building could pick up a portion of such delayed photons and possibly provide a dramatic signal. In fact, we will demonstrate that sensitivity to GMSB models with substantial $\tilde{\chi}_1^0$ decay length will be maximized by implementing all three (OHC, b, RA) delayed-decay signals.

We will now outline the results we have obtained for these signals and the associated procedures. Events were generated simultaneously for all SUSY production mechanisms by modifying ISASUGRA/ISAJET [24] to incorporate the GMSB boundary conditions, and then forcing delayed $\tilde{\chi}_1^0$ decays according to the predicted $c\tau$. We used the toy calorimeter simulation package ISAPLT. We simulated calorimetry covering $|\eta| \leq 4$ with a cell size given by $\Delta R \equiv \Delta\eta \times \Delta\phi = 0.1 \times 0.0875$ and took the hadronic (electromagnetic) calorimeter resolution to be $0.7/\sqrt{E}$ $(0.15/\sqrt{E})$. The D0 electromagnetic calorimeter was simplified to a thin cylinder with radius $r = 1$ m and length $-2\ \text{m} \leq z \leq +2$ m. Also important to the analysis was the central outer hadronic D0 calorimeter OHC, which we approximated as occupying a hollow solid cylinder defined by $-2\ \text{m} \leq z \leq +2$ m and radial region $2\ \text{m} \leq r \leq 2.5$ m. It is important that the D0 OHC is segmented in ΔR and that there are also several layers of inner hadronic calorimeter.

The signals are defined in terms of jets, isolated leptons, isolated prompt photons and isolated delayed-decay photons (i.e. emerging from $\tilde{\chi}_1^0$ decays occurring with substantial delay).

(i) A jet is defined by requiring $|\eta_{\text{jet}}| < 3.5$ and $E_T^{\text{jet}} > 25$ GeV (for $\Delta R_{\text{coal.}} = 0.5$).

(ii) An isolated lepton is defined by requiring $|\eta_{\ell}| < 2.5$ and $E_T^{\ell} > 20$, 15, 10 GeV for the most energetic, 2nd most energetic and 3rd most energetic lepton, respectively.[3] The criterion for isolation is $E_T(\Delta R \leq 0.3) < 4$ GeV (summing over all other particles in the cone surrounding the lepton).

(iii) A photon is a prompt-photon candidate if it emerges from a $\tilde{\chi}_1^0$ decay that occurs before the $\tilde{\chi}_1^0$ has reached the electromagnetic calorimeter. The $(\eta_\gamma, \phi_\gamma)$ of such a photon is defined by the direction of the vector pointing from the interaction point to the point at which it hits the electromagnetic calorimeter. (This is generally not the same as the direction of the photon's momentum.) An isolated prompt photon is defined by requiring $|\eta_\gamma| < 1$ and $E_T^\gamma > 12$ GeV, with isolation specified by $E_T(\Delta R \leq 0.4) < 4$ GeV, summing over all other particles in the cone surrounding the point at which the photon hits the EM calorimeter. Photons that emerge within the hollow cylinder defined by the electromagnetic calorimeter, but that are not isolated, are merged with hadronic jets as appropriate.

(iv) An isolated delayed-decay OHC signal photon is defined as one that emerges from a $\tilde{\chi}_1^0 \to \gamma\tilde{g}_{3/2}$ decay that takes place inside an OHC cell and that has $E_T^\gamma > 15$ GeV, with isolation specified by $E_T(\Delta R \leq 0.5) < 5$ GeV, summing over all other particles in the cone surrounding the location of the $\tilde{\chi}_1^0$ decay. This implies, in particular, that there should be very little energy deposited in the inner hadronic calorimeter cells in the same (η,ϕ) location as the OHC cell in which the $\tilde{\chi}_1^0$ decay occurs.

(v) An isolated delayed-decay impact-parameter signal photon is defined as one that emerges from a $\tilde{\chi}_1^0 \to \gamma\tilde{g}_{3/2}$

[3]We never consider more than three isolated leptons, and all leptons are prompt.

decay (occurring before the $\tilde{\chi}_1^0$ has exited the tracking region) and that passes through the central electromagnetic calorimeter (with the dimensions and physical location specified earlier). The photon is required to have $E_T^\gamma > 15$ GeV. No isolation requirement is imposed. Nor is there any specific requirement on the apparent rapidity (i.e. as measured by the location at which it passes through the electromagnetic calorimeter).

(vi) A delayed-decay roof-array signal photon is defined as one that emerges from a $\tilde{\chi}_1^0 \to \gamma \tilde{g}_{3/2}$ decay that occurs at a vertical distance in the range 6.5 m$<z<$16.5 m from the interaction point and has $E_T^\gamma > 15$ GeV. This means that the $\tilde{\chi}_1^0$ will have decayed past the muon detector system but below the roof of the D0 detector building. The delayed-decay photon is required to pass through a 28 m$\times$38 m rectangle centered at 16.5 m above the interaction point. This is the approximate size of roof array that could be positioned so that no part of the array would have a large amount of material between it and the 6.5 m height referred to earlier. No further isolation requirements or other cuts are placed on the photon.

We now give the specific requirements for each type of signal. First, for all signals, events are retained only if at least one of several sets of reasonable trigger requirements are satisfied. The triggers considered were the following.

(1) $\not\!\!E_T > 35$ GeV.

(2) four or more jets with $E_T^{\rm jet} > 15$ GeV.

(3) (a) two or more jets with $E_T^{\rm jet} > 30$ GeV; (b) $\not\!\!E_T > 40$ GeV.

(4) (a) one or more leptons with $E_T^{\ell} > 15$ GeV, $|\eta_\ell| < 2.5$ and isolation defined by $E_T(\Delta R < 0.3) < 5$ GeV; (b) $\not\!\!E_T > 15$ GeV.

(5) (a) two or more leptons with $E_T^{\ell} > 15$ GeV, $|\eta_\ell| < 2.5$ and isolation defined by $E_T(\Delta R < 0.3) < 5$ GeV; (b) $\not\!\!E_T > 10$ GeV.

(6) two or more photons with $E_\gamma > 12$ GeV, $|\eta_\gamma| < 1$ and isolation specified by $E_T(\Delta R < 0.4) < 4$ GeV.

The additional signal-specific cuts are itemized below.

The standard jets-plus-missing-energy signal. We employ D0 cuts [21]: (a) $n(\text{jets}) \geqslant 3$—labelled $k = 1,2,3$ according to decreasing E_T; (b) no isolated $[E_T^{\rm had.}(\Delta R \leqslant 0.3) < 5$ GeV] leptons with $E_T > 15$ GeV; (c) $\not\!\!E_T > 75$ GeV; (d) $0.1 < \Delta\phi(\not\!\!E_T, j_k) < \pi - 0.1$ and $\sqrt{(\Delta\phi(\not\!\!E_T, j_1) - \pi)^2 + (\Delta\phi(\not\!\!E_T, j_2))^2} > 0.5$. The background cross section level has been estimated by D0 to be $\sigma_B = 2.35$ pb. The signal will be deemed observable if: (i) there are at least 5 signal events, (ii) $\sigma_S/\sigma_B > 0.2$, and (iii) $N_S/\sqrt{N_B} > 5$, where N_S and N_B are the numbers of signal and background events.

The tri-lepton signal. We employ the cuts of Ref. [26]: three isolated leptons, $n(\text{jets}) = 0$, $\not\!\!E_T > 25$ GeV and $|M(\ell_i \ell_j) - m_Z| > 8$ GeV $(i \neq j)$. For these cuts, the cross section for the sum of all backgrounds to the tri-lepton signal is $\sigma_B = 0.2$ fb.

The tri-lepton-plus-prompt-photon signal. We impose the same cuts as for the tri-lepton signal, but require in addition that there be at least one prompt photon (as defined above) present. We shall presume that the background to this signal will be negligible. This seems reasonable given the already quite small background to the simple tri-lepton signal.

The two-prompt-photon-plus-missing-energy signal. Following Ref. [15], we require: (a) at least two isolated prompt photons (as defined above); and (b) $\not\!\!E_T > \not\!\!E_T^{\rm min}$. Detection efficiency of 80% (100%) is assumed if $E_T^\gamma < 25$ GeV (> 25 GeV). This signal should be completely free of background provided $\not\!\!E_T^{\rm min}$ is adjusted appropriately as a function of luminosity. The signal will be deemed observable if there are 5 or more events.

The delayed-neutralino-decay signal resulting when the $\tilde{\chi}_1^0$ decay takes place in the outermost hadronic calorimeter cell of the D0 detector. In an event in which a $\tilde{\chi}_1^0 \to \gamma \tilde{g}_{3/2}$ decay occurs inside one of the outer hadronic calorimeter (OHC) cells, the γ will deposit all its energy in the cell. By demanding substantial γ energy and isolation (precise requirements were given earlier) for this deposit, along with other criteria, backgrounds can be made small.[4] More specifically, we require that the event fall into one of three classes defined by the following sets of requirements:

(1) (a) $n(\text{jets}) \geqslant 3$; (b) at least one delayed-decay OHC photon; (c) $\not\!\!E_T > \not\!\!E_T^{\rm min}$.
(2) (a) any number of jets; (b) two or more delayed-decay OHC photons; (c) $\not\!\!E_T > \not\!\!E_T^{\rm min}$.
(3) (a) any number of jets; (b) at least one prompt photon; (c) at least one delayed-decay OHC photon; (d) $\not\!\!E_T > \not\!\!E_T^{\rm min}$.

In the absence of the needed detector-specific study, we will assume zero background to $1.+2.+3.$ for the same $\not\!\!E_T^{\rm min}$ values that will be employed for the prompt-2γ signal. Observability of the delayed-decay OHC signal is assumed if the number of events for $1.+2.+3.$ is 5 or more. Of the above three sub-signals, 1. provides by far the largest event rates in the moderate $\sqrt{F}$ region.

The impact-parameter signal. We require $n(\text{jets}) > 3$, $\not\!\!E_T > \not\!\!E_T^{\rm min}$ and one or more delayed-decay impact-parameter photons (as defined above) with transverse impact parameter b larger than 2 cm. The D0 detector in run-II will have a pre-shower installed and is expected [27] to achieve a 1σ resolution of about 0.2 cm in the transverse impact parameter. Thus, our 2 cm requirement amounts to a 10σ deviation from zero impact parameter. We assume zero background and require $\geqslant 5$ events for observability.

The roof-array signal. We require $n(\text{jets}) > 3$, $\not\!\!E_T > \not\!\!E_T^{\rm min}$ and one or more delayed-decay roof-array photons. If there is directionality or timing for the roof array, additional cuts that ensure tiny backgrounds could be incorporated without significant losses in the signal event rate. However, such additional cuts are not imposed in this study. As above, we assume zero background after cuts and require $\geqslant 5$ events for observability.

[4]Our additional criteria will be chosen so that the cross section for producing an isolated energetic long-lived kaon in association therewith is small. Further, any such kaon will interact strongly and is almost certain to be absorbed before reaching the OHC.

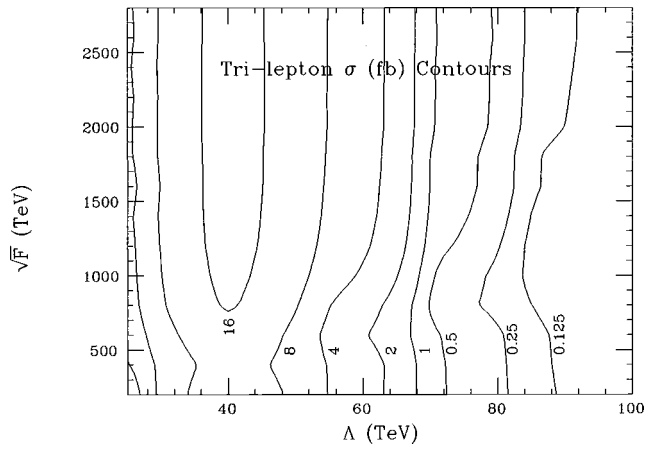

FIG. 2. We present cross section contours in fb units for the tri-lepton signal (as defined in the text).

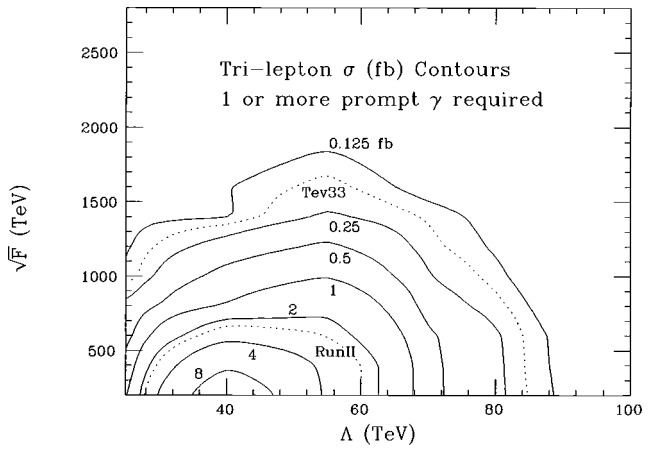

FIG. 3. We present cross section contours in fb units for the tri-lepton-plus-prompt-photon signal (as defined in the text). In addition to the cuts for the tri-lepton signal, we impose the requirement that there be at least one prompt photon present. The solid contours are the same ones presented in Fig. 2. The dotted contours correspond to 5 events at Tev33 ($L=30$ fb^{-1}) and 5 events in run-II ($L=2$ fb^{-1}).

We will now summarize our results for all these channels. A limited subset of these results appeared in Ref. [18]. In the present paper, our discussion will focus on the luminosities expected in run-II and at TeV33.[5] We begin with the jets-plus-missing-energy and tri-lepton signals.

The jets-plus-missing-energy-signal. Employing the cuts specified above, for $L=0.1$ fb^{-1} (run-I), we found in Ref. [18] that this signal was viable for any $\sqrt{F}$ if $\Lambda \lesssim 25$ TeV. For both $L=2$ fb^{-1} and $L=30$ fb^{-1}, the signal is viable for any $\sqrt{F}$ if $\Lambda \lesssim 30$ TeV. Given the lower bound of ~ 55 TeV coming from the lower bound on $m_{\tilde{\gamma}_R}$, it would appear that the jets-plus-missing-energy signal will not be useful at the Tevatron.

The tri-lepton signal. Contours of constant cross section for this signal are presented in Fig. 2. Compared to the background cross section, $\sigma_B=0.2$ fb, we see that in order to achieve $S/\sqrt{B}=5$, we require a signal cross section of $\sigma=8.4$ fb at $L=0.1$ fb^{-1} (run-I), $\sigma=1.6$ fb at $L=2$ fb^{-1} (run-II) and a signal cross section of $\sigma=0.41$ fb at $L=30$ fb^{-1} (Tev33), respectively. Figure 2 then shows that the parameter space for which supersymmetry can be discovered using this signal extends to $\Lambda \sim 50$ TeV for $L=0.1$ fb^{-1}, to $\Lambda \sim 65$ TeV for $L=2$ fb^{-1} and to $\Lambda \sim 75$ TeV for $L=30$ fb^{-1}. Thus, the tri-lepton discovery mode will allow supersymmetry detection out to substantially higher Λ than does the jets plus missing energy mode. (This is to be expected since the tri-lepton signal tends to be stronger than the jets-plus-missing-energy signal at Fermilab Tevatron energies [26].) In particular, it can probe above the ~ 55 TeV lower bound on Λ coming from CERN e^+e^- LEP-2 limits on $m_{\tilde{\gamma}_R}$.

For both these signals, we should note that if $\sqrt{F}$ is small enough then, in association with the jets or leptons, one will detect prompt photons (coming from the decays of the $\tilde{\chi}_1^0$'s that are inevitably present). The prompt-two-photon signal to be discussed below will also be in evidence. There will then be little doubt that nature has chosen a GMSB model rather than a supergravity (SUGRA)[6] model with similar boundary conditions for the gaugino and sfermion soft-supersymmetry-breaking masses. However, if $\sqrt{F}$ is large there will be no prompt photons and no hint for the GMSB character of the model from these two signals. To illustrate these points, we turn to the prompt-photon signals.

The tri-lepton-plus-prompt-photon signal. Contours of constant cross section for this signal are presented in Fig. 3. The solid contours are the same as plotted in Fig. 2. The dotted contours correspond to 5 events at Tev33 ($\sigma=0.16$ fb at $L=30$ fb^{-1}) and 5 events in run-II ($\sigma=2.5$ fb at $L=2$ fb^{-1}). Five events should be adequate for discovery given the negligible background expected. We observe that prompt photons will be seen in association with the tri-lepton signal only for $\sqrt{F} \lesssim 600$ TeV at $L=2$ fb^{-1} and only for $\sqrt{F} \lesssim 1600$ TeV at $L=30$ fb^{-1}.

We now turn to the impact-parameter (b), outer-hadronic-calorimeter (OHC), roof-array (RA) and prompt-two-photon (2γ) signals. In all these cases, we shall presume that our cuts can be chosen so as to eliminate any back-

[5]We will not discuss the delayed-decay signals for run-I luminosity here. The OHC signals give only a marginal increase in the range of parameter space for which a supersymmetry signal might emerge for the low $L \sim 100$ pb^{-1} integrated luminosity accumulated in that run. Only if the stringent cuts we employ for the delayed-decay OHC signals could be weakened without encountering backgrounds would present data allow elimination of a significant additional portion of parameter space. Background studies are now in progress [25]. The impact-parameter and roof-array signals cannot be implemented for the run-I data set.

[6]As usual, the SUGRA acronym refers to models in which supersymmetry breaking in a hidden sector is transmitted to the supersymmetric partners of the SM particles by gravitational interactions rather than gauge interactions. The gravitino in such models is heavy and an LSP $\tilde{\chi}_1^0$ is stable in the absence of R-parity violation.

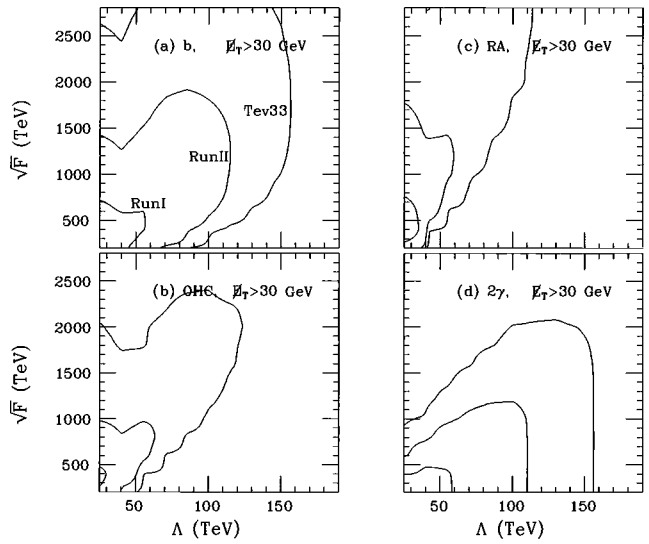

FIG. 4. We present cross section contours in the $(\sqrt{F},\Lambda)$ parameter space for the (a) impact-parameter (b), (b) outer-hadronic (OHC), (c) roof-array (RA), and (d) prompt-two-photon (2γ) signals. Contours are given at $\sigma=0.16$, 2.5, and 50 fb (the outermost contour corresponding to the smallest cross section, *etc.*). We note that $\sigma=0.16,2.5,50$ fb corresponds to 5 events at $L=30,2,0.1$ fb^{-1}, respectively. Hence the labels Tev33, run-II and run-I, respectively. In this figure we have taken $\not\!\!E_T^{\rm min}=30$ GeV for all signals. Other jet and photon requirements are as specified in the text.

ground. In particular, we will consider cross sections and event rates for the cuts stated earlier with various choices of $\not\!\!E_T^{\rm min}$. A complete summary of our simulations is contained in Figs. 4, 5, and 6, where we give cross section contours for the above signals in the $(\sqrt{F},\Lambda)$ parameter space for $\not\!\!E_T^{\rm min}=30$, 50 and 70 GeV, respectively.

We now discuss the implications of the results contained in Figs. 4, 5, and 6.

The prompt-2γ signal. Based on the background results of [22] (see also [23]) and eye-ball extrapolations thereof, we

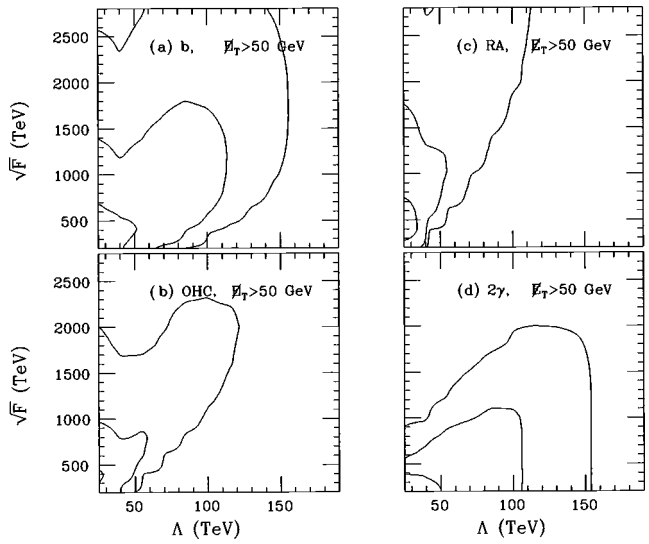

FIG. 5. Same as in Fig. 4, but for $\not\!\!E_T^{\rm min}=50$ GeV.

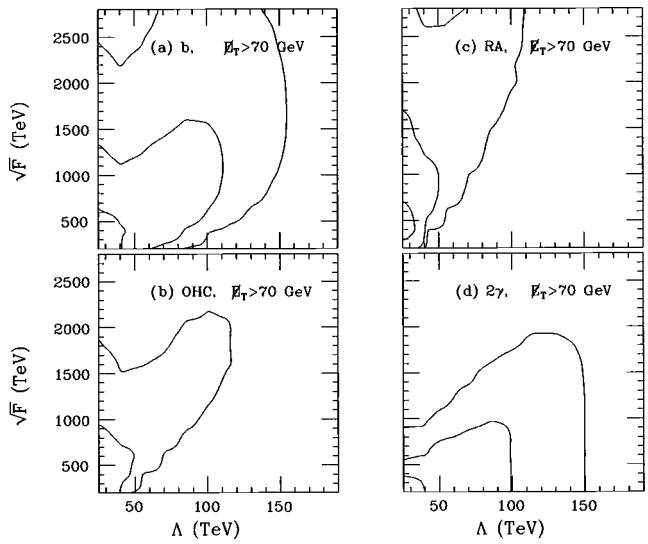

FIG. 6. As in Fig. 4, but for $\not\!\!E_T^{\rm min}=70$ GeV.

estimate that our jet requirements and photon energy/isolation requirements are such that $\not\!\!E_T^{\rm min}=30$, 50, 70 GeV is sufficient to eliminate all background for luminosities of $L=100$ pb^{-1}, 2 fb^{-1}, 30 fb^{-1}, respectively. Thus, to ascertain the discovery reach of this channel for $L=100$ pb^{-1}, one refers to the $\sigma=50$ fb contour of Fig. 4. For $L=2$ fb^{-1}, one refers to the $\sigma=2.5$ fb contour of Fig. 5; and for $L=30$ fb^{-1}, one refers to the $\sigma=0.16$ fb contour of Fig. 6. From these contours, we conclude that the signal is viable in a region described as follows. For $L=2$ fb^{-1}, the region extends from small $\sqrt{F}$ up to $\sqrt{F}\sim 600$ TeV if $\Lambda\lesssim 35$ TeV, increasing to $\sqrt{F}\sim 1000$ TeV at $\Lambda\sim 80-100$ TeV; the signal is not viable beyond $\Lambda\sim 100$ TeV. For $L=30$ fb^{-1}, the region extends from small $\sqrt{F}$ up to $\sqrt{F}\sim 900$ TeV if $\Lambda\lesssim 35$ TeV, increasing to $\sqrt{F}\lesssim 1000$ TeV at $\Lambda\sim 120-130$ TeV; the signal is not viable beyond $\Lambda\sim 150$ TeV.

The OHC signal(s). We provisionally adopt the same $\not\!\!E_T^{\rm min}$ cuts of $\not\!\!E_T^{\rm min}=30$, 50, 70 GeV for $L=100$ pb^{-1}, 2 fb^{-1}, 30 fb^{-1}, respectively, as employed for the prompt-2γ signal. Assuming that 5 events are sufficient (i.e. that the background is negligible for our other strong cuts on jets and photon energy/isolation) to give an observable signal, we look at the same σ contours as a function of L as in the prompt-2γ case, with the following results. For $L=2$ fb^{-1}, the OHC signal provides a useful, but not enormous, extension of the region of parameter space for which supersymmetry can be detected as compared to the portion of parameter space covered by the prompt-two-photon signal or jets-plus-missing-energy signal. This extension is mainly in the $\sqrt{F}\lesssim 800-1000$ TeV, $\Lambda\lesssim 50$ TeV region. Of course, we noted earlier that CERN e^+e^- collider LEP-2 data probably already excludes this Λ region. For $L=30$ fb^{-1}, the reach of the OHC signal is greatly extended; supersymmetry detection may be possible via the OHC signal for essentially all of the $\sqrt{F}\lesssim 1500-2000$ TeV, $\Lambda\lesssim 120$ TeV portion of parameter space for which the prompt-two-photon signal is not viable. Conversely, supersymmetry detection at the low-$\sqrt{F}$

points at large Λ for which the OHC signal falls below 5 events would be possible via the prompt-2γ channel. In addition, there is a substantial region in which both these signals are viable. Since the tri-lepton signal only extends out to about $\Lambda \lesssim 75$ TeV for $L=30$ fb^{-1}, it is apparent that, at the Tev33 luminosity, the prompt-2γ and OHC signals combine to significantly extend to higher values of Λ, the region where supersymmetry can be detected. In particular, Λ values substantially beyond the approximate limit of $\Lambda \gtrsim 55$ TeV coming from CERN e^+e^- collider LEP-2 data can be probed.

We make two further remarks regarding the OHC signals.

(1) Of the three delayed-decay OHC signals, the first ($\geqslant 3$ jets$+\geqslant 1$ OHC γ) is observable (i.e. yields at least five events) for the entire $(\sqrt{F},\Lambda)$ region where the OHC signals are shown to be viable. The second ($\geqslant 2$ OHC γ's) yields $\geqslant 5$ events for only a very small portion of this region. The third ($\geqslant 1$prompt $\gamma+\geqslant 1$ OHC γ) yields $\geqslant 5$ events for the lower (roughly, half) $\sqrt{F}$ portion of the region for which the combined OHC signals are viable.

(2) If simulations eventually show that the first OHC signal is background-free for smaller $\not{E}_T^{\rm min}$ than employed here (as we are hopeful will be the case), the portion of parameter space for which it is viable expands; e.g. using $\not{E}_T^{\rm min}=50$ GeV at $L=30$ fb^{-1}, the $\geqslant 5$ event region would extend to $\sqrt{F}\sim 1800-2300$ TeV for $\Lambda \lesssim 120$ TeV.

The impact-parameter signal. Requiring $\not{E}_T^{\rm min}=50,70$ GeV at $L=2,30$ fb^{-1}, respectively, Figs. 5 and 6 show that the b signal has an even larger region with $\geqslant 5$ events than does the OHC signal. For $L=2$ fb^{-1}, one finds 5 or more events for $\sqrt{F}\lesssim 1200-1700$ for $\Lambda \lesssim 115$ TeV. For $L=30$ fb^{-1}, one finds 5 or more events for $\sqrt{F}\lesssim 2200-3000$ TeV for $\Lambda \lesssim 150$ TeV. Only in a small corner with small $\sqrt{F}$ and large Λ does the b signal fail, and this region is handily covered by the prompt-2γ signal. As compared to the tri-lepton signal, the impact-parameter signal extends to substantially higher Λ values for $\sqrt{F}\lesssim 1600$ TeV at $L=2$ fb^{-1} and for $\sqrt{F}\lesssim 2700$ TeV for $L=30$ fb^{-1}.

In comparing Figs. 4, 5 and 6 we can see that weakening the $L=30$ fb^{-1} missing energy cut to $\not{E}_T^{\rm min}=50$ GeV results in a slight increase in the $\geqslant 5$ event parameter space region. Weakening the cut still further to $\not{E}_T^{\rm min}=30$ GeV appears (we cannot be precise since our scan did not extend to high enough $\sqrt{F}$) to result in a substantial increase to higher $\sqrt{F}$ of the $\geqslant 5$ event region.

The roof-array signal. For $L=2$ fb^{-1}, the RA signal has $\geqslant 5$ events up to $\sqrt{F}\lesssim 1500$ TeV for $\Lambda \lesssim 40$ TeV. In all of this region, the tri-lepton and impact-parameter signals, but not the tri-lepton-plus-prompt-photon signal, will also be viable. For $L=30$ fb^{-1}, the RA signal has $\geqslant 5$ events for large $\sqrt{F}\lesssim 2800-3000$ TeV when $\Lambda \lesssim 120$ TeV. This Λ reach at high $\sqrt{F}$ is substantially greater than achieved by the tri-lepton signal. As $\sqrt{F}$ decreases, the Λ extent of the $\geqslant 5$ event region decreases.

In comparing Figs. 4, 5 and 6 we can see that weakening the $L=30$ fb^{-1} cut to $\not{E}_T^{\rm min}=50$ GeV, or, if possible without encountering backgrounds, $\not{E}_T^{\rm min}=30$ TeV, substantially increases the high $\sqrt{F}$ reach of the $\geqslant 5$ event region for $\Lambda \lesssim 120$ TeV.[7]

One especially important point regarding the delayed-decay signals discussed above is the following. If $\sqrt{F}$ is large, they are the only signals that will allow one to ascertain that nature has chosen a GMSB model, even if supersymmetry is detected in the jets-plus-missing-energy and/or tri-lepton modes. In particular, we saw above that the tri-lepton-plus-prompt-photon and prompt-two-photon signals will not be in evidence at large $\sqrt{F}$, regardless of the magnitude of Λ. Without the delayed-decay signals, a SUGRA model with GMSB-like boundary conditions for the soft-supersymmetry-breaking masses of the gauginos and sfermions would then be indistinguishable from a GMSB model with a large value for $\sqrt{F}$.

The dependence of our signals on various energy variables may be useful in designing triggers and considering backgrounds. To this end, we present a figure showing the distributions in E_γ, $E_T^{\rm jet}$ and $\not{E}_T$ for the impact-parameter and roof-array signals. These distributions are presented for the parameter space point $\sqrt{F}=1400$ TeV and $\Lambda=50$ TeV; they are fairly representative of the results obtained at other parameter space points. In these distributions, we have imposed a more limited set of cuts.

(1) In the case of the distributions presented for the impact-parameter signal, we require only that there be one or more delayed-decay impact-parameter photon (as defined earlier) with $b>2$ cm, except that when plotting the E_γ distribution, we remove the cut on E_γ.

(2) In the case of the distributions presented for the roof-array signal, we require only that there be one or more delayed-decay roof-array photons (as defined earlier).

In neither case do we impose jet cuts, except that when plotting $d\sigma/dE_T^{\rm jet}$, the jets must satisfy the definition of a jet as given earlier. In addition, no cuts are placed on $\not{E}_T$. In the case of the $E_T^{\rm jet}$ and E_γ distributions, all jets and delayed-decay (impact-parameter in the first case, and roof-array in the second case) photons satisfying the minimum requirements noted above are included in the histograms.

From the plots of Fig. 7 we observe the following.

(1) Our E_γ cuts accept essentially all events and could be strengthened somewhat without significant loss of signal event rate.

(2) The $E_T^{\rm jet}$ spectrum is falling very rapidly, and it would be undesirable to strengthen the jet cuts unless it is absolutely necessary.

(3) Cuts significantly stronger than $\not{E}_T^{\rm min}>70$ GeV will start to cause a significant loss of signal rate. Thus, we hope that such a stronger cut will not be needed to eliminate backgrounds.

It is also potentially important to know how sensitive the impact-parameter signal is to the impact-parameter resolu-

[7]Since our parameter scan was limited to $\sqrt{F}\lesssim 2800$, we are unable to be quantitative in this statement.

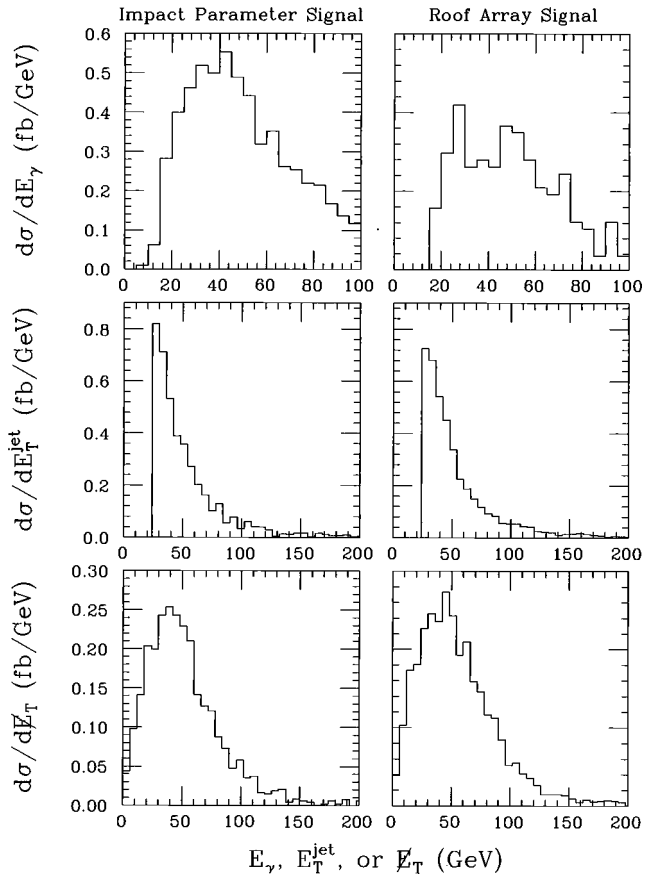

FIG. 7. For the impact-parameter and roof-array signals, we plot $d\sigma/dE_\gamma$, $d\sigma/dE_T^{\rm jet}$ and $d\sigma/d\not{E}_T$ for the parameter space point $\sqrt{F}=1400$ TeV and $\Lambda=50$ TeV. The limited cuts applied are described in the text.

tion. To this end, we present in Fig. 8 the same cross section contours for the impact-parameter signal as given in Fig. 5 (for $b>2$ cm), for the cases (a) $b>50$ cm and (b) $b>10$ cm, keeping all other cuts (including $\not{E}_T^{\rm min}=50$ GeV) the same. We observe that the b cut can be increased from 2 cm to 10 cm without significant damage to the signal. But, if the transverse impact parameter resolution were as poor as the 5 cm–10 cm resolution applicable [27] during run-I (for which the D0 detector did not have a pre-shower device) a cut of $b>50$ cm would probably be needed to eliminate backgrounds and the region of viability of the impact-

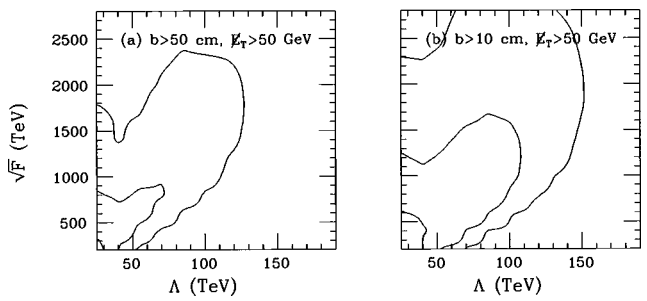

FIG. 8. For $\not{E}_T>50$ GeV, we plot the same cross section contours for the impact-parameter signal as given in Fig. 5 (for $b>2$ cm), for the cases (a) $b>50$ cm and (b) $b>10$ cm. All other cuts are identical.

parameter signal would decrease very substantially. In fact, for all cases $[(L=100\ {\rm pb}^{-1},\not{E}_T^{\rm min}=30\ {\rm GeV})$, $(L=2\ {\rm fb}^{-1},\not{E}_T^{\rm min}=50\ {\rm GeV})$ and $(L=30\ {\rm fb}^{-1},\not{E}_T^{\rm min}=70\ {\rm GeV})]$ the region for which ≥ 5 events are found for the impact-parameter signal after requiring $b>50$ cm is quite similar to that for which ≥ 5 OHC signal events are found. In contrast, the region for which ≥ 5 impact-parameter signal events are expected for the $b>10$ cm or $b>2$ cm cuts is always substantially larger than the region for which ≥ 5 OHC signal events are predicted in all the above three $(L,\not{E}_T^{\rm min})$ cases.

III. DISCUSSION AND CONCLUSIONS

We have studied a simple gauge-mediated supersymmetry breaking model in which the lightest neutralino, the $\tilde{\chi}_1^0$, is the next-to-lightest supersymmetric particle and decays to photon plus gravitino. The model is characterized by the parameters Λ (which sets the scale of the masses of the superpartners of the standard model particles) and $\sqrt{F}$ (which specifies the scale at which supersymmetry is broken in the hidden sector and, thereby, determines the mass of the gravitino and the lifetime of the $\tilde{\chi}_1^0$). We have argued that it is very possible (indeed, preferred in the simplest existing GMSB models) for the $\sqrt{F}$ parameter to be sufficiently big that there is a large probability for the $\tilde{\chi}_1^0$ to decay a substantial distance from the interaction point. We have shown that the portion of the $(\sqrt{F},\Lambda)$ parameter space for which a signal for supersymmetry can be seen at the Fermilab Tevatron is greatly expanded by employing signals sensitive to such delayed decays.

In particular, it is useful to compare (a) the standard SUSY signatures (jets plus missing-energy or three leptons plus missing-energy), (b) the prompt-two-photon signal and (c) the delayed-decay (impact-parameter, roof-array and outer-hadronic-calorimeter) signals.

(1) Of the standard SUSY signatures, the tri-lepton signal is the stronger. Using it, discovery of GMSB supersymmetry will be possible for small to moderate Λ values, $\lesssim 65$ ($\lesssim 75$ TeV) at run-II (Tev33), regardless of the size of $\sqrt{F}$.

(2) The prompt-two-photon signal is viable for small to moderate $\sqrt{F}$, but extending to reasonably large Λ, $\Lambda \lesssim 100$ TeV ($\lesssim 150$ TeV) at run-II (Tev33).

(3) The delayed-decay signals are potentially viable in the large-$\sqrt{F}$, large-Λ portion of parameter space not covered by the standard SUSY and prompt-two-photon signals. For run-II, the delayed decay signals could allow supersymmetry discovery for all of $\sqrt{F}\lesssim 1700$ TeV, $\Lambda\lesssim 100$ TeV, extending at Tev33 to cover essentially the entire $\sqrt{F}\lesssim 3000$ TeV and $\Lambda \lesssim 120$ TeV region that is preferred in the context of the model we have explored.[8]

[8]In a more general GMSB model, it is certainly possible that the entire interesting region of parameter space might not be accessible using the delayed-decay signals. Still, we expect that the delayed-decay signals will always significantly expand the amount of GMSB parameter space at larger $\sqrt{F}$ for which a supersymmetry signal can be discovered.

If $\sqrt{F}$ is large, the delayed-decay signals will be important even if Λ is in the small to moderate range ($\Lambda \lesssim 65-75$ TeV) for which the standard jets-plus-missing-energy and/or tri-lepton SUSY signatures will be visible. This is because the prompt-photon signals (tri-lepton-plus-prompt-photon or prompt-two-photon) will not be in evidence if $\sqrt{F}$ is big. Without employing the impact-parameter, roof-array and/or outer-hadronic-calorimeter delayed-decay signals there will be no hint that nature has chosen a GMSB model, as opposed to a SUGRA model with GMSB-like boundary conditions for gaugino and sfermion soft-supersymmetry-breaking masses.

If delayed decay signatures are seen, the next goal will be to determine the parameters of the GMSB model. These include the all important value of $\sqrt{F}$ and the masses of the supersymmetric particles. The latter will allow us to determine the overall scale Λ and the relative sizes of the soft-supersymmetry-breaking masses as a function of Λ. Important input information will include: (a) the distribution of $\tilde{\chi}_1^0$ decays as a function of distance from the interaction point, as reflected in the relative rates for different signals (e.g. the prompt-two-photon rate as compared to the roof-array rate), (b) the energy distribution of the photons from the $\tilde{\chi}_1^0$ decays, (c) the time at which the photons from the $\tilde{\chi}_1^0$ decays arrive at various elements of the detector (e.g. the electromagnetic calorimeter pre-shower, the outer-hadronic-calorimeter cell or the roof-array), (d) the missing-energy distribution, and (e) the types of different particles that appear in association with the supersymmetric events, and their energy distributions. All of these depend in a complicated way on the parameters of interest. For example, the distance distribution of $\tilde{\chi}_1^0$ decays, the photon energies, and the timing of the photons from the decays all depend strongly on $(c\tau)_{\tilde{\chi}_1^0}$ and $m_{\tilde{\chi}_1^0}$, and might allow their determination.[9] Even a rough measurement of these latter two quantities will allow us to estimate $\sqrt{F}$ using Eq. (8). Further, the energy distributions of the visible particles (jets, leptons, and photons) will reflect both the relative and absolute masses of the sparticles. For example, thresholds reflecting $m_{\tilde{\ell}_R} - m_{\tilde{\chi}_1^0}$ and/or $m_{\tilde{\ell}_L} - m_{\tilde{\chi}_1^0}$ might show up in lepton energy distributions. And so forth. Obviously, substantial statistics will be required for a relatively model-independent determination of $\sqrt{F}$ and the soft-supersymmetry-breaking masses.

We note that all the delayed-decay signals we considered here are potentially useful for any model in which the decay of the $\tilde{\chi}_1^0$ is not prompt. For example, in R-parity violating (RPV) SUGRA models the RPV couplings may be sufficiently small that the $c\tau$ for $\tilde{\chi}_1^0$ decay is quite substantial. The products emerging from the $\tilde{\chi}_1^0$ decay (whether three leptons, one lepton plus two jets, or three jets) can emerge in the outer hadronic calorimeter, with large impact parameter, or outside the detector and pass through the roof array. There is also the possibility that R-parity violation could be present in GMSB models. For an appropriate balance between the magnitude of $\sqrt{F}$ and the size of the RPV couplings, the $\tilde{\chi}_1^0$ could have prominent decays both to RPV channels and to $\gamma\tilde{g}_{3/2}$, and both types of $\tilde{\chi}_1^0$ decays could be substantially delayed. In general, observation of the delayed-decay signals would be quite critical to determining the relative branching ratios for RPV and $\gamma\tilde{g}_{3/2}$ decays of the $\tilde{\chi}_1^0$. A similar set of remarks would apply to RPV (SUGRA or GMSB) models in which a right-handed slepton is the lightest of the superpartners of the SM particles.[10] Thus, the utility of the types of delayed-decay signals we propose will extend far beyond the NLSP$=\tilde{\chi}_1^0$, R-parity-conserving GMSB model context analyzed in detail here.

Our study has focused on using the D0 detector in the configuration planned for run-II, with the addition of a (relatively cheap) roof-array detector. There are, of course, much more ambitious possibilities in which a decay volume and special detector, specifically designed to pick up delayed $\tilde{\chi}_1^0$ decays, is constructed some distance from the main detector. Nonetheless, since the delayed-decay photon signals discussed here show great promise and since delayed decays in general could easily prove to be the hallmark signature of gauge-mediated supersymmetry breaking, not to mention R-parity violation, the CDF and D0 detector groups should work to clarify and refine these signals and, in particular, the backgrounds thereto.

ACKNOWLEDGMENTS

This work was supported in part by the U.S. Department of Energy under Grant No. DE-FG03-91ER40674, and by the Davis Institute for High Energy Physics. We are grateful to B. Dobrescu, H. Murayama, and S. Thomas for helpful conversations. We particularly wish to acknowledge important conversations with S. Mani regarding the D0 detector and the possibility of implementing the delayed-decay signals discussed here.

[9] As an example, one could measure the time of flight of the $\tilde{\chi}_1^0$ to the OHC cell (by the time of the OHC energy deposit) and the energy of the deposit (*i.e.* the energy of the photon). The flight time is a function of $c\tau$, $m_{\tilde{\chi}_1^0}$ and the average $\tilde{\chi}_1^0$ energy. The photon energy is a function of the latter two. The correlation between the flight time and photon energy (as measured in a large number of events) might allow a roughly model-independent determination of $c\tau$ and $m_{\tilde{\chi}_1^0}$.

[10] The main difference, as compared to the $\tilde{\chi}_1^0$ case, is that additional information would arise from observation of the visible track associated with a semi-stable charged $\tilde{\ell}_R$. Also, a long-lived $\tilde{\ell}_R$ might be absorbed inside the detector.

[1] M. Dine and A. E. Nelson, Phys. Rev. D **48**, 1277 (1993); M. Dine, A. E. Nelson and Y. Shirman, *ibid.* **51**, 1362 (1995); M. Dine, A. E. Nelson, Y. Nir and Y. Shirman, *ibid.* **53**, 2658 (1996).

[2] N. Arkani-Hamed, J. March-Russell and H. Murayama, Nucl. Phys. **B509**, 3 (1998); H. Murayama, Phys. Rev. Lett. **79**, 18 (1977); K.-I. Izawa, Y. Nomura, K. Tobe and T. Yanagida, Phys. Rev. D **56**, 2886 (1997); M. Luty, Phys. Lett. B **414**, 71 (1997); Y. Nomura and K. Tobe, Phys. Rev. D **58**, 055002 (1998).

[3] S. Dimopoulos, S. Thomas and J. D. Wells, Nucl. Phys. **B488**, 39 (1997).

[4] P. Fayet, Phys. Lett. **70B**, 461 (1977); **86B**, 272 (1979); **175B**, 471 (1986).

[5] N. Cabibbo, G. R. Farrar and L. Maiani, Phys. Lett. **105B**, 155 (1981); M. K. Gaillard, L. Hall and I. Hinchliffe, *ibid.* **116B**, 279 (1982); J. Ellis and J. S. Hagelin, *ibid.* **122B**, 303 (1983); D. A. Dicus, S. Nandi and J. Woodside, Phys. Lett. B **258**, 231 (1991).

[6] H. Pagels and J. R. Primack, Phys. Rev. Lett. **48**, 223 (1982); T. Moroi, H. Murayama and M. Yamaguchi, Phys. Lett. B **303**, 289 (1993); S. Borgani, A. Masiero and M. Yamaguchi, *ibid.* **386**, 189 (1996).

[7] A. de Gouvea, T. Moroi and H. Murayama, Phys. Rev. D **56**, 1281 (1997).

[8] See, for example, P. Dornan, ALEPH Status Report, 1997, http://alephwww.cern.ch/ALPUB/seminar/lepc/LEPCnov97.html.

[9] T. Goto and M. Yamaguchi, Phys. Lett. B **276**, 103 (1992); E. J. Chun, H. B. Kim and J. E. Kim, Phys. Rev. Lett. **72**, 1956 (1994).

[10] T. Han and R. Hempfling, Phys. Lett. B **415**, 161 (1997).

[11] J. F. Gunion, in *Future High Energy Colliders*, Proceedings of the ITP Symposium, Santa Barbara, California, 1996, edited by Z. Parsa (AIP, New York, in press), pp. 41–64, hep-ph/9704349.

[12] S. Raby, Phys. Rev. D **56**, 2852 (1997); Phys. Lett. B **422**, 158 (1998).

[13] S. Dimopoulos, M. Dine, S. Raby and S. Thomas, Phys. Rev. Lett. **76**, 3494 (1996).

[14] S. Ambrosanio, G. Kane, G. Kribs, S. Martin and S. Mrenna, Phys. Rev. Lett. **76**, 3498 (1996).

[15] H. Baer, M. Brhlik, C.-H. Chen and X. Tata, Phys. Rev. D **55**, 4463 (1997).

[16] J. Bagger, K. Matchev, D. Pierce and R.-J. Zhang, Phys. Rev. Lett. **78**, 1002 (1997).

[17] S. Martin, Phys. Rev. D **55**, 3177 (1997).

[18] C.-H. Chen and J. F. Gunion, Phys. Lett. B **420**, 77 (1998).

[19] CDF Collaboration, S. Park, in *10th Topical Workshop on Proton–Antiproton Collider Physics*, edited by R. Raja and J. Yoh (AIP, New York, 1995).

[20] D0 Collaboration, B. Abbott *et al.*, Phys. Rev. Lett. **80**, 442 (1998); E. Flattum (for the CDF and D0 Collaborations), Report No. FERMILAB-Conf-97/404-E.

[21] D0 Collaboration, S. Abachi *et al.*, Phys. Rev. Lett. **75**, 618 (1995).

[22] D0 Collaboration, S. Abachi *et al.*, Phys. Rev. Lett. **78**, 2070 (1997).

[23] CDF Collaboration, D. Toback *et al.*, Report No. FERMILAB-Conf-96/240-E.

[24] F. Paige and S. Protopopescu, in *Supercollider Physics*, edited by D. Soper (World Scientific, Singapore, 1986), 41; H. Baer, F. Paige, S. Protopopescu and X. Tata, in *Argonne Accelerator Physics* (1993), pp. 703–720.

[25] D0 Collaboration, S. Mani *et al.* (work in progress).

[26] H. Baer, C.-H. Chen, C. Kao and X. Tata, Phys. Rev. D **52**, 1565 (1995).

[27] D0 Collaboration, G. Landsberg *et al.* (private communication).